EXPERIMENTS TO STUDY MESON RESONANCES

A. R. Clark
Lawrence Radiation Laboratory

G. Conforto
University of Chicago

V. P. Kenney
University of Notre Dame

A. W. Key
National Accelerator Laboratory

H. A. Neal
Indiana University

and

J. Pine
California Institute of Technology

ABSTRACT

A bubble chamber-spark chamber-counter "hybrid" system, a counter-spark chamber system and a missing-mass spectrometer are discussed as possible approaches to the study of meson resonances at NAL energies. The basic reaction considered is $\pi + N \rightarrow \pi + \pi + \pi + N$. We have tried to limit the size and complexity of the apparatus required, so as to be appropriate for an experiment during the initial operation of the NAL accelerator.

I. INTRODUCTION

As part of the NAL 1969 Summer Study Program, this group has looked into various methods for studying meson resonances.

We have tried to limit the size and complexity of the apparatus required so as to be appropriate for an experiment during the initial operation of the NAL accelerator.

For a reaction of the type

$$\text{meson} + \text{nucleon} \rightarrow \text{meson resonance} + \text{nucleon},$$

the types of experiments to be done can be perhaps broken down, in order of decreasing available information, into three categories:

1. Study of the Production Cross Section. The properties of the resonance are known and one wants to study the production cross section as a function of s (square of c.m. energy) and t (square of four-momentum transfer to the nucleon). Experiments of this type clearly need to cover ranges in s and t as large as possible, but do not necessarily need a large acceptance for detecting the decay products of the resonance.

2. Study of the Properties of a Resonance. The resonance is only known to exist and one wants to determine its properties. Experiments of this type need only to produce as copiously as possible the resonance to be studied and can accept very limited s and t ranges. The properties of the produced resonance are investigated by:

a. determining the branching ratios of the various possible decay modes,

b. measuring the angular distributions in the decays of the resonance, and

c. measuring the angular distributions in the decays of the decay products of the resonance.

For these types of experiments, it is clearly desirable to have:

a. an acceptance for primary and secondary decay products as large as possible (including neutrals), and

b. a sure mass identification of the primary and secondary decay products.

3. Search for New Resonances. This is just "bump hunting"--one needs to cover, in several steps if necessary, a rather large mass (i.e., s) range, and it is of course convenient to have, for rate considerations, a rather good t acceptance.

In principle, very little attention needs to be given to decay products. In practice, however, some identification of the final states may very well be necessary, since total cross sections remain practically constant with increasing energy while resonance production cross sections decrease and the problem of detecting bumps becomes more and more difficult. Since one is not attempting to measure angular distributions, large biases in the acceptance of the decay products can be tolerated.

It is quite clear from the above considerations that an apparatus designed to perform experiments of type 1 will also be resonably well suited for experiments of type 3, but, in general, will be of rather limited usefulness for carrying out experiments of type 2.

II. EXPERIMENTAL DESIGN

As a specific example of such an apparatus, we have tried to design an experiment to study the reaction:

$$\pi^{\pm} + p \rightarrow \pi^{\pm} + \pi^{+} + \pi^{-} + p, \qquad (1)$$

under the assumptions that the momentum transfer to the proton is low and that the process will proceed by diffractive dissociation of the incident pion. The apparatus, and much of the design study, is applicable to peripheral production of meson resonances in general, but we have not pursued the possibilities for measurement of other reactions in detail. The experiment aims to provide data on the following attributes of the process:

a. The s dependence of the cross section.

b. The t dependence of the cross section.

c. The mass spectrum of the three-pion final state.

We have investigated three possible experiment arrangements:

a. A "hybrid" system utilizing a bubble chamber plus a wire-chamber spectrometer for fast forward particles.

b. A system with a liquid hydrogen target and counter-spark chamber arrays replacing the bubble chamber in the preceding system.

c. A recoil missing-mass spectrometer, with associated counters for detecting outgoing mesons and measuring their angles.

Arrangements (a) and (b) rely primarily on measurements of the outgoing pion momenta and angles to determine the mass of the pion system; the recoil proton provides additional constraints in some kinematic regions. Arrangement (c) relies on the kinematics of the slow recoil proton. In all three cases, we provide for detection of both charged particles and gamma rays. This feature provides a relatively clean trigger and eliminates (in principle) the need to detect missing particles by kinematic constraints, and in turn reduces the accuracy required of measurements on the outgoing particles.

Some considerations on setups specifically intended for experiments of type 2 and 3 are also presented.

III. KINEMATICS FOR $\pi + p \rightarrow X + p$

Minimum 4-Momentum Transfer to the Proton

For diffraction dissociation, the differential cross section is expected to behave in the same manner as for diffractive elastic scattering:

$$\frac{d\sigma}{dt} \sim e^{-b|t|},$$

with the constant b approximately equal to 10 $(\text{BeV})^{-2}$. We have assumed that the

production cross section of any resonance in the reaction $\pi + p \rightarrow X + p$ follows this law. In addition, the diffractive dissociation cross section has been assumed to be energy-independent, in contrast to the cross sections for peripheral processes from meson exchange which decrease approximately as p_0^{-2}.

For production of a resonance of mass M_x, the following approximate formula is valid provided the recoil momentum of the proton is small and the incident beam momentum p_0 is much greater than M_x:

$$|t_{min}| \approx \frac{1}{4} \frac{M_x^4}{p_0^2} .$$

The recoil proton kinematics are related to the momentum transfer t by the relation

$$T_p = \frac{|t|}{2M} ,$$

where T_p is the proton kinetic energy and M is the proton mass. For small values of the recoil proton momentum p_p, such that $p_p << M$, this can be approximated by

$$p_p \approx |t|^{1/2} .$$

Figure 1 shows $p_{p\,min}$ vs M_x for beam momenta of 50 and 100 GeV/c.

To obtain a usable cross section in the diffractive region, we should have $t_{min} \leq (M_\pi^2) \approx 0.02$; the formulae above then determine maximum values of M_x which can be effectively observed for various beam momenta:

p_0 (BeV/c)	M_x (BeV)
50	3.8
100	5.3
150	6.6

If we can observe recoil protons up to some cutoff momentum p_{max}, with a corresponding t_{max}, the fraction of the total cross section which is observed is

$$\frac{\Delta\sigma}{\sigma} = \int_{t_{min}}^{t_{max}} \frac{d\sigma}{dt}\, dt \Big/ \int_{t_{min}}^{\infty} \frac{d\sigma}{dt}\, dt .$$

This quantity is plotted as a function of p_{max} in Fig. 2, where we have used $d\sigma/dt$ as given above and set $t_{min} = 0$.

Decay Kinematics for M_x (Aperture Required for Fast Forward Particles)

Figures 3 and 4 show the kinematics for the decay $M_x \to 2\pi$, which provide a useful guide for the decays to $\pi + \rho$ and to 3π; for fast forward particles and for $M_x \gtrsim 2$ GeV the 2π kinematics are a very good approximation to the $\pi\rho$ kinematics. Figure 5 shows kinematics for $\rho \to 2\pi$.

For M_x decays to 3π, we can estimate from Figs. 3, 4, and 5 that a forward cone of 10 degrees half-angle will give ~ 2π solid angle for $M_x = 2$ BeV with $p_0 = 50$ BeV/c, and $M_x = 4$ BeV with $p_0 = 100$ BeV/c.

Mass Resolution for the 3-Pion System

The mass M_x can be determined from the momenta and angles of the three outgoing pions via the relation:

$$M_x^2 = \left(E_1 + E_2 + E_3\right)^2 - \left(\vec{p}_1 + \vec{p}_2 + \vec{p}_3\right)^2 .$$

For high pion momenta, and small angles between the pions, this relation leads to the simple approximation:

$$M_x^2 = 3M_\pi^2 + p_1 p_2 \theta_{12}^2 + p_2 p_3 \theta_{23}^2 + p_3 p_1 \theta_{13}^2 ,$$

with an obvious notation. In order to get a simple estimate of the accuracy with which M_x is determined in a typical case, we will assume $M_x^2 >> 3m_\pi^2$ and a perfectly symmetric decay with $p_1 = p_2 = p_3 = (1/3)p_0$ and $\theta_{12} = \theta_{23} = \theta_{31} = \theta$. We then find, assuming that the three terms involved in determining M_x^2 have uncorrelated errors,

$$\frac{\Delta M_x}{M_x} \approx \left[\frac{2}{3}\left(\frac{\Delta p}{p}\right)^2 + \frac{1}{3}\left(\frac{\Delta\theta}{\theta}\right)^2 \right]^{1/2} .$$

From this special example, a momentum accuracy of 1.4% and an opening-angle accuracy of 1% lead to an uncertainty in the mass M_x of about 1%. For a less symmetric case in which all momenta and angles are measured with these precisions, we estimate a mass resolution perhaps a factor 2 worse.

As an example, suppose we have an incident momentum p_0 of 90 BeV/c and a mass M_x of 3 BeV decaying to three pions, each with 30 BeV/c. Then the angle θ is about 50 milliradians. A spectrometer which can measure momenta of 30 BeV/c to 1.7%, and angles to 0.5 milliradians is not terribly difficult to achieve, and the mass accuracy is quite adequate for a first experiment. Such a spectrometer is discussed in more detail in Sections III and IV.

Recoil Proton Kinematics for M_x

Measurements of the angle and momentum of the recoil proton and the incident pion are sufficient to determine M_x; some kinematic relations for 100-BeV incident pions are shown in Fig. 6. It can be seen that for θ near 0 degrees, the mass is determined basically by the proton momentum. In this case the range of t for a given mass and a given value of s is very limited. However, in the region from about 30 to 70 degrees, a reasonable range of t is accessible for masses in the range 3 to 6 BeV. For masses less than about 2 BeV, the measurement of the proton momentum and angle will not yield satisfactory accuracy in M_x. However, since $p_{p\,min}$ scales as $(p_0)^{-1/2}$, some extension to lower masses will occur at 50 BeV.

From the kinematics, it appears that a proton missing-mass-spectrometer may be a useful tool for studying moderately high masses with a limited range of s and t for each value of the mass. (See Section VI.)

IV. A HYBRID BUBBLE CHAMBER-SPARK CHAMBER SYSTEM

Layout of the System

Figure 7 shows a possible experimental layout for a hybrid bubble chamber-spark chamber system. The rapid cycling bubble chamber allows direct observation of the interaction region and gives good measurements on slow and/or wide angle charged secondary particles. The fast charged final-state particles are analyzed with a spectrometer consisting of magnet M2 and sets of wire planes to measure the entrance and exit angles. The magnet M2 is to provide a BL product of about 30 kG-meters, or a transverse momentum of about 1 BeV/c.

The aperture of magnet M2 subtends a rectangular cone measuring ~±6 by ±12 degrees. This aperture seems like a reasonable compromise between cost and event rate. The parameters of magnet M2 are:

length × width × height--1.5 m × 2.5 m × 1.5 m

field--20 kG.

The main dimensions of the bubble chamber and magnet are listed in Table I. The chamber will use bright-field optics and an omega bellows expansion system. A conservative estimate of the total thickness of the exit window is 1/2 in. aluminum; hopefully it can be made thinner. Its size is determined by the acceptance of the spectrometer. The magnet gap need not be 0.4 m all around; the coil can be a solenoid with a downstream hole. (See Fig. 8.)

The array of scintillation counters labeled H in Fig. 7 forms a two-dimensional counter hodoscope which will be used to determine the number of charged particles entering the spectrometer. For the reaction under study, the hodoscope outputs will

Table I.

Bubble-chamber diameter	1 m
Bubble-chamber height	1 m
Exit-window dimension (L × H)	60 cm × 30 cm
Magnetic field	40 kG
Magnet inner diameter	1.5 m
Downstream magnet gap	0.4 m

be used as part of the master trigger to guarantee that only those events with three charged final state particles are recorded.

Gamma-ray counters are used after the spectrometer to veto those events with unwanted π^{o}'s. Also, counters to detect gamma rays may be needed to subtend most of the solid angle around the bubble chamber. The downstream detectors could be a large array of lead-lucite Cerenkov shower counters, and would not be particularly expensive or difficult to construct.

Accuracy

A study of the kinematics of the reaction $\pi + p \rightarrow 3\pi + p$ indicates that at an incident beam momentum of 50 BeV/c, the momenta of the pions produced at angles outside a ±12 degree cone are $\lesssim$ 7 BeV/c. (See Fig. 3.) The bubble chamber will measure the momenta of these particles to sufficient accuracy. The accuracy attainable with the bubble chamber is shown in Fig. 9.

The momenta of the faster particles in the forward cone will be measured in the downstream spectrometer. The entrance angle of a 30 BeV/c particle into the spectrometer can be measured to ±0.2 mrad using a combination of spark-chamber and bubble-chamber position measurements. At the downstream end, the angle can be determined to ±0.5 mrad with the spark chambers as shown. Multiple scattering in the air is negligible at this momentum. Thus, at 30 BeV/c, assuming a spark chamber resolution of 0.3 mm, a $\Delta p/p$ of ±1.6% can be achieved. Thus, for measurements with three fast forward pions, the spectrometer should lead to a mass accuracy $\Delta M_x/M_x$ of ~ 1.5% at incident energies up to about 100 BeV.

It should be noted that the requirements on the accuracy of measurement on the relatively low momentum pions which are to be measured in the bubble chamber are probably not as severe as the approximations of Section II would imply. In the asymmetric case, two pions will carry off the majority of the energy, and the uncertainty in mass determination will be dominated by the errors in the momenta of these two pions. However, it is clear from Fig. 9 that a 40 kG field is required to attain an

accuracy approaching that required up to 7 BeV/c. Since measurement of all four particles from the interaction will provide a four constraint fit, the final fitted errors will in fact be about 70% of the raw measurement errors.

As far as angular accuracy is concerned, the bubble chamber can attain $\Delta\theta/\theta \lesssim 1\%$ for pions outside the ±12 degree cone down to momenta of about 1 BeV/c. Above 7 BeV/c the angular accuracy is dominated by the measurement error with $\Delta\theta \sim 0.75$ mrad; the multiple scattering in 1/2 meter of H_2 is negligible in this region, and information from the downstream spectrometer will be used, as discussed above.

It is worth noting that some additional information comes from the measurement of the recoil proton. For protons produced at large angles in the laboratory, M_x is quite well determined for values above about 4 BeV; however, as pointed out by Walker[1] the resolution is hopeless at lower masses. This matter is discussed more fully below in the section on the missing mass spectrometer.

Rates

Table II gives measured cross sections for πp interactions at 20 BeV/c[2] and some estimates for 60 and 120 BeV/c. Assuming that the chamber provides a useful interaction length of 1/2 m of liquid, with ten expansions per pulse, ten tracks per expansion, and 15 pulses per minute, we see about 2×10^6 beam particles per day, with the rates per day shown in the table. It is assumed that the full 4π solid angle is covered.

Table II.

Process	20 BeV	60 BeV	120 BeV	Rate per day at 60 BeV
σ_{Total}	25 mb	25 mb	25 mb	100K
4-Prong	8 mb	5 mb	3 mb	20K
$p\pi^+\pi^-\pi^+$	0.9 mb	0.5 mb	0.3 mb	2K
p "A"	0.15 mb	0.15 mb	0.15 mb	600

For a 1 microbarn cross section, the rate drops to about 4 events per day. Thus, the rate calculations indicate that the chamber is adequate for studying diffraction dissociation but will be rather poor for individual non-diffractive final states (like ρN^*) which are expected to have cross sections on the order of a few microbarns.

The substitution of a smaller chamber running at a higher repetition rate will improve the data-taking rate; however, a smaller chamber will be unable to achieve the accuracy required here.

Triggering

In studying a bubble-chamber system, we felt that if the chamber provided a useful rate for the diffraction dissociation process it would in addition provide a rich variety of other data. The by-product data would of course depend on the effectiveness of trigger arrangements or upon an ability to effectively scan a large number of pictures taken with loose triggering.

It is fairly simple to design a downstream trigger on an interacting beam particle, or to require two or three particles in the downstream spectrometer. It should be noted that it is extremely helpful to have beam spark chambers or a hodoscope ahead of the bubble chamber, both to improve the knowledge of the incident particle and to indicate which beam particle has interacted, particularly if a sweeping magnet is used. A measuring machine such as POLLY can then operate very efficiently in the automatic scan-measure mode.

It would be extremely useful to have a veto on gamma rays from unwanted π^o's produced in the chamber. It is very awkward to cover the top and bottom of the chamber, due to the cameras and the expansion system respectively. However, it seems quite feasible to place large yet inexpensive lead-lucite Cerenkov shower counters around the walls of the chamber. The gammas in a ±12 degree cone escape through the thin exit window and are detected behind the downstream spectrometer. For high energies the shower counters discriminate easily between gammas and pions; unfortunately the large angle particles will tend to be a relatively low energy and the detectors are not quite so effective. Some wide angle gammas will also escape detection by interacting in the walls of the chamber itself, so it appears that we cannot effectively veto all events with π^o's.

For the reaction discussed here, the kinematics appear to save the situation. If we can be certain that the downstream veto has eliminated the need to consider π^o's in the forward cone, the transverse momentum is sufficiently well determined to detect the presence of a missing neutral particle unless it has very low momentum or is produced almost directly backwards in the laboratory. Using the figures given in Section II.3, at an incident momentum of 90 BeV/c, the contribution to the transverse momentum uncertainty of one charged pion from the decay of the X is approximately:

$$p\,\delta\theta \sim \frac{90}{3} \cdot \frac{1}{100} \cdot 50 \cdot 10^{-3} \sim 15 \text{ MeV/c.}$$

At low t values the proton momentum can be measured to ~ 5 MeV/c, giving a total error in the transverse momentum of approximately 25 MeV/c.

However, this conclusion implies only that we can separate multi-π^0 events from 4c fits after they have all been photographed and fully measured, and this is not an effective way to achieve high statistics on a particular reaction.

The good ionization discrimination of the bubble chamber will be extremely useful in scanning for events with a slow proton, and the vertex visibility will be extremely useful in rejecting events which gave a false trigger. Again, however, this is not true triggerability.

Discussion and Conclusions

The advantages of the bubble chamber in this system include its ability to see the vertex, to measure momenta and angles of the low energy pions to good precision, and to identify some particles with its good ionization discrimination.

However, it has many disadvantages. Rates are low, even for the relatively abundant process being studied here. It is very difficult to devise satisfactory triggering. Finally, the duty cycle of presently-available bubble chambers (~ 100 msec cycle time at best) is a poor match to the rest of the spectrometer system. There is no solution to this fundamental problem, at least with present technology. The experiments at Wisconsin and SLAC with chambers that cycle at 50-90 cps, and hopefully faster, look promising. Standing-wave bubble chambers are still pretty much in the future.

We conclude that the main advantage of the bubble chamber is its ability to see all topologies in a relatively unbiased way. The ability to see exactly which tracks left the vertex in the bubble chamber greatly facilitates our determination of trigger biases in the downstream spectrometer. The usefulness of the bubble chamber is greatly decreased when we restrict the analysis to a single channel.

V. A HYDROGEN TARGET AND SPARK-CHAMBER ARRAY AS AN ALTERNATIVE TO THE BUBBLE CHAMBER

In Fig. 10, a sketch of a target and surrounding counters and spark chambers is shown which is intended to provide information about particles emerging from the target at large angles and to provide a vertex determination. The main reason for considering such a system as an alternative to the bubble chamber is to increase the counting rate, to allow more complete coverage with gamma veto counters and to ease the task of establishing a trigger scheme for a particular reaction.

For simplicity, the array is intended to detect low energy recoil protons in only half the total azimuth, utilizing spark chambers and counters on both sides of the target. The wire chambers are for measuring angles, while the dE/dx and E scintillators are to identify protons and measure their energy. (The E scintillator is

like one which has been studied at Northeastern University[3] which provides a resolution of about 1% at a proton energy of about 150 MeV.)

The shower counters around the target are used to detect π^o's; these counters need to be efficient for low energy gammas, so it is probably easiest to use lead-scintillator sandwiches. These counters would also detect wide angle charged pions, but not recoil protons which stop in the E counter.

The forward angle spectrometer to be used with this system is shown in Fig. 10. The magnet is identical with the one in the hybrid system (2.5 m wide × 1.5 m high × 1.5 m long, 20 kG field). The spark chambers which measure the decay angles of the forward pions are spaced by 2.5 m, which with a spark chamber resolution of ±0.3 mm gives an angular uncertainty $\Delta\theta = \pm 0.2$ mrad. The exit angle from the magnet is measured to $\Delta\theta = \pm 0.5$ mrad with chambers at 1 m spacing. These angular errors result in momentum and opening angle measurement errors consistent with those discussed in Section II on kinematics, giving a mass error $\Delta M_x/M_x \approx 1\%$.

The last spark chamber is followed by a hodoscope and a lead-lucite Cerenkov shower-counter. In contrast to the shower counters around the target, this shower counter must not detect charged pions--hence the choice of a lead-lucite Cerenkov counter. Since the gammas entering this counter tend to have high energies, this type of counter can easily differentiate between gammas and pions.

In order to study the reaction $\pi^\pm + p \to \pi^\pm + \pi^+ + \pi^- + p$, a trigger could be composed as follows:

$$\text{Trigger} = (\text{Beam})\,(\text{Proton})\,(\text{Spectrometer})\,(\overline{\text{Shower Counters}}),$$

where "Beam" involves the presence of a properly identified incident pion; "Proton" means proper dE/dx and E signals for a proton stopping in E; "Spectrometer" signifies three charged particles detected in the downstream spectrometer hodoscope; and "Shower Counters" means a signal in any shower counter.

This apparatus provides a solid angle of about $4\pi/10$ steradians for the process

$$\pi^\pm + p \to p + \pi^\pm + \pi^+ + \pi^-,$$

or for other peripheral meson resonance production processes. The "nonforward" mesons from the resonance decay, which the bubble chamber would measure, will be vetoed here unless a "medium energy spectrometer" is considered worthwhile adding. The target is assumed to be a 5 mm diameter cylinder, 30 cm long, which takes advantage of the small beam divergence and size expected at NAL. We believe that the total material between the hydrogen and the dE/dx counter can consist mainly of about 0.010 in. of mylar, and if this is the case, protons of momentum greater than

about 140 MeV/c emitted at lab angles greater than 45 degrees can trigger the apparatus. This gives $\gtrsim 80\%$ efficiency for detecting diffraction dissociation.

For the three-pion diffraction dissociation process, this apparatus should provide a rate increase of a factor of 500 over the bubble chamber plus spectrometer system discussed in Section III. This is based on a rather arbitrary beam intensity of 10^6 pions per pulse, which should be available. Clearly, for peripheral processes with large cross sections ($\gtrsim$ 100 microbarns) this target array can be useful with a more modest downstream spectrometer subtending a smaller solid angle than the one proposed in the previous section for use with the bubble chamber. Alternatively, with the proposed spectrometer, this apparatus can provide rates of the order of 1000 events per day for peripheral processes with cross sections of one microbarn.

The trigger proposed above is basically designed to select recoil protons with momentum less than about 700 MeV/c (determined by when they penetrate to the veto behind the E counter) and to veto on any additional particles. However, the variety of triggering arrangements made possible by reorganizing the electronics should provide useful solid angles for many other reactions. We have not gone into this question in detail, but it seems clear that when running such a device a number of different triggers can be used in parallel to simultaneously study more than one reaction. The apparatus will then also reflect a multiplicity of interests, and probably differ from that shown in Fig. 9.

A few examples of relatively low cross-section processes that can be studied are:

a. $\pi^- + p \rightarrow X^o + N^*$, where X^o is a neutral system decaying to two charged particles in the forward cone (a ρ meson or a high mass member of the ρ trajectory for example). The target triggering would then require a proton from the N^* in one quadrant containing E and dE/dx counters, and a pion in the opposite quadrant, or more likely in any of the other three quadrants.

b. $\pi^+ + n \rightarrow X^o + p$, a reaction in which a deuterium target is used to produce an all-charged final state, the X^o decaying into charged particles.

c. $\pi^- + p \rightarrow X^o + n$, similar to the preceding reaction, but with a proton target. Scintillators surrounding the target are all placed in veto, and neutron counters subtending some reasonable solid angle are needed. The E counters, with dE/dx and shower counters in veto, may be quite useful neutron detectors.

Finally, it should be mentioned that the apparatus can function as a missing-mass spectrometer with good resolution for proton momenta between about 400 and 700 MeV/c. Just as with the bubble chamber, there will be a momentum range

(somewhat smaller here) within which the recoil proton and the downstream spectrometer are both effective in determining the mass of the forward pion system.

VI. MISSING-MASS SPECTROMETER

The kinematics for the reaction

$$\pi + p \rightarrow X + p,$$

for a beam momentum of 100 BeV are plotted in Fig. 6. They show that the mass of X can be determined by measuring the angle θ_p and the momentum p_p of the recoil proton.

Two regions of the θ_p, p_p plane are particularly interesting:

a. The "Jacobian peak" region is which $\delta M_x/\delta p_p \approx 0$, where M_x can be determined by measuring θ_p only.

b. The "0-degree" region in which $\delta M_x/\delta \theta_p \approx 0$, where M_x can be determined by measuring p_p only.

As mentioned in Section V, the region of interest for p_p is roughly $300 \leq p_p \leq 500$ MeV/c. The lower limit is dictated by the fact that very low energy protons will either not emerge from a liquid hydrogen target or they will undergo such large multiple scattering that a measurement of their direction is almost useless. This limit can be lowered considerably if it is possible to use a gaseous hydrogen target. The upper limit is dictated by the fact that the resonance production cross section for $p_p > 500$ MeV/c is negligible.

The Jacobian peak and the 0 degree regions have substantially different characteristics and will be discussed separately.

The Jacobian Peak Region

The choice of the beam momentum and the condition $\delta M_x/\delta p_p = 0$ determine the mass region which can be usefully covered. For example, for a π beam momentum of 100 BeV/c, the point where M_x is rigorously independent of the proton momentum is $M_x = 3.6$ BeV. In practice, with this choice of the beam momentum, it is possible to cover the range $3.2 \leq M_x \leq 4.0$ BeV with $\delta M_x/\delta p_p \approx 0$. This is achieved by detecting the recoil proton in the angular region

$$65° \leq \theta_p \leq 72°,$$

(see Fig. 6).

The correspondence between the beam momentum and the useful mass region make this trigger best suited for experiments of type 2, as discussed in Section I. The X's produced are relatively low mass and this tends to confine their decay products in the forward hemisphere, thus giving a good start towards the possibility of

observing an unbiased decay angular distribution. For example, Fig. 4 shows that the decay products of a particle of mass M_x = 4 BeV with a momentum of 100 BeV/c are all confined in a forward cone of ±36° aperture.

If the 100 BeV/c incoming beam has a momentum bite $\Delta p/p \lesssim 0.3\%$, the mass resolution is dominated by the uncertainty in the measurement of the proton angle introduced by multiple scattering. Assuming an average multiple scattering angle of ±3.5 mrad, the mass resolution is ±1%. The practical realization of a suitable proton detector (except for the further limitation $65° \leq \theta_p \leq 72°$) has been discussed in Section V.

It is worth mentioning that this mass resolution can also be obtained in the case in which the recoil baryon is a neutron. The angular region to be covered is only ±3.5° or ±60 mrad; a neutron detector 1.2 meters long, capable of locating the interaction point of the neutron to ±3.5 cm placed at 10 meters from the target would be adequate. Such a detector could consist, for instance, of a plastic scintillator in which the interaction location is determined from the difference in the time of flight of the light in the scintillator to photomultipliers at the two ends.

Since the mass and the momentum of X are accurately known from the production reaction, two-body decays ($\pi\pi$, $K\bar{K}$, $\eta\pi\ldots$) and three-body decays ($\pi\pi\pi$, $\eta\pi\pi$, $K\bar{K}\eta\ldots$) of X can be reconstructed, with 2c and 1c fits respectively, from the measured directions of charged particles and γ rays emitted in the decay or in subsequent decays of the decay products. In this case only a weak large-aperture magnet to determine signs of charged particles may be necessary. Angles of final state particles can be measured to ±0.5 mrad without much difficulty. For a two-pion decay of X, this allows us to determine center-of-mass (c.m.) angles to about ±1° and lab momenta to about ±1.8%. There is not much point in measuring directions with better accuracy since the uncertainties in M_x and p_x (determined from the recoil proton) introduce ~±0.5 mrad uncertainty in the correlation between lab and c.m. angles. Similar considerations presumably hold for three-body decays of X.

In the example considered here, and for all two and three-body decays, it is clear from Fig. 4 that:

1. If all the decay products of X are charged, it is not too difficult to detect them all in a forward detector of reasonable aperture. The problem of vetoing unwanted π^o's is also rather simple since, if no particle from the X decay is emitted backward in the laboratory, the γ-ray counters discussed in Section V need cover only the forward hemisphere.

2. If one wants to study the X decay modes involving π^o's by detecting both

γ rays from their decays, an unbiased efficiency requires essentially a 4π geometry. Detection of γ rays in a $\sim \pm 60°$ aperture cone in the forward direction is needed to insure that there is no π^o from X decay for which the efficiency for detecting both γ's is zero. The problem of dealing with π^o's can, in some cases, be avoided, since it is always possible to increase the charge of X by one unfit, by detecting neutron instead of a proton in the production reaction. This is not applicable to $\eta \rightarrow \gamma + \gamma$ decays which are, however, rather well collimated forward.

For X decays into more than three particles, a system capable of measuring only directions is clearly inadequate. However, for the same missing mass, as more particles are produced, or as the decay products become more massive, the more they tend to go forward. For example if a X of 100 BeV/c with a mass of 3.6 BeV decays into $K\bar{K}$, both K's are contained in a cone of $\sim \pm 7°$. Although clearly a more detailed study of this question is necessary, it seems quite feasible to attempt to detect a good fraction, if not all, of the charged particles from X decays in a forward spectrometer where momenta as well as directions are measured with good accuracy. One is, therefore, reduced to a scheme similar to the one discussed in Section V in order to investigate states of higher multiplicity.

A spectrometer accepting all charged products of X in the forward direction is also very useful in identifying final states. In fact the M_x determined from the decay of X by the magnetic spectrometer depends on the assumptions made about the masses of the particles detected, whereas the M_x determined from the production of X by the missing-mass spectrometer does not. This provides a check on the assumption made for the decay mode of X.

The expected rates are essentially those discussed in Section V. At least an order of magnitude reduction with respect to these estimates is to be expected for neutron detection.

In conclusion, a "Jacobian peak" trigger on protons or neutrons assoicated with a downstream apparatus capable of measuring (1) direction of charged particles and γ rays over a large forward solid angle (about $\pm 40°$ for charged particles and $\pm 60°$ for γ rays), and (2) directions and momenta of charged particles and directions of γ rays in a more restricted forward region (like the one described in Section V) looks very suitable for performing a rather large class of experiments described as type 2 in Section I.

A sketch of a possible setup is presented in Fig. 12. The forward magnetic spectrometer preforms the functions described in detail in Section V. Directions of charged particles or γ rays not accepted by the magnetic spectrometer are measured at larger angles. The constraint on the recoil proton angle insures that no pion (or

heavier particle) from X decay is emitted backward. Events in which two or three charged particles are detected in the field free region can be reconstructed with a 2c or 1c fit respectively. The apparatus has a low but non-zero efficiency for detecting both γ's from the slowest π^0 in the decay of X. The efficiency for detecting η's from X decays via the decay $\eta \rightarrow \gamma + \gamma$ is rather good.

The Zero-Degree Region

Figure 6 shows that, for the same beam momentum, much higher masses are explored in this region than in the Jacobian peak region. The mass of X is determined by the momentum of the proton, and the constraint $300 \leq p_p \leq 500$ MeV/c couples the beam momentum to the mass region explored. Any given X is observed with its lowest kinematically possible momentum transfer and therefore the highest production cross section. Figure 4 shows that the decay products of X can easily go backward in the laboratory.

These facts clearly indicate that a zero-degree missing-mass spectrometer is a very good match to experiments described as type 3 in Section I.

In principle, the apparatus consists only of a low-field magnetic spectrometer capable of measuring the momentum of the recoil proton. In practice, in order to increase the signal-to-noise ratio, at least some rough identification of final states will probably be necessary. This does not seem too difficult to accomplish, since, because of the nature of the experiment performed, it is only necessary to do this in a limited region of the angular distribution.

For a π beam of 100 BeV/c, the accessible mass region is $7.2 \leq M_x \leq 8.7$ BeV (see Fig. 6). With a beam momentum bite of $\Delta p/p = 0.3\%$ and assuming a 1% resolution in the measurement of the recoil proton momentum, the mass resolution in this region turns out to be $\lesssim 0.5\%$.

With a π beam of 10^6 π per pulse and with a 30 cm liquid hydrogen target, event rates are of the order of one event every ten pulses for a 1μb cross section.

VII. BEAM REQUIREMENTS

The experiments described in Sections V and VI above (all spark-chamber systems) require a beam with the following properties:

Particles	π^-, π^+
Momentum	50, 100 BeV/c
Flux	10^6 particles/accel. pulse
Spill length	1 sec
Final image	1 mm × 1 mm
Divergence at final focus	≤ 2.5 mrad
$\Delta p/p$	not critical

The spot size and divergence are set by the condition that the beam must pass through a hydrogen target of dimensions 5 mm diameter × 30 cm long. Spark chambers will be used ahead of the target to measure the angle of the incident particle. If the required flux can be obtained with $\Delta p/p \leq 0.1\%$, no additional measurements of the incident momenta is required; if $\Delta p/p > 0.1\%$, spark chambers will also be used ahead of the last beam dipole to measure the momentum. The π^+ beam will require a Cerenkov counter in the beam.

Discussions with people in the summer study's Beam Group indicate that the above requirements can be easily satisfied at the 200-BeV accelerator.

The hybrid system described in Section IV requires the following beam:

Particles	π^-
Momentum	50, 100 BeV
Flux	10^2 particles/accel. pulse
Expansion/accel. pulse	10
Particles/Expansion	10
$\Delta p/p$	$\leq 0.1\%$

Two different beam conditions could be used by the bubble chamber:

1. The beam could be focused in the chamber and stepped across the entrance window with a sweeping magnet during each expansion; or

2. The necessary separation of the 10 beam particles/expansion could be achieved by defocusing the beam horizontally in the chamber.

In either case the angle and identification of the interacting particle would be measured with hodoscopes or spark chambers in the beam.

Operation with incident π^+ would require a separated beam.

VIII. CONCLUSIONS AND COMMENTS

1. We believe that we have demonstrated that at least first round experiments can be done with conventional techniques and with relatively simple equipment. The advantages and disadvantages of the three arrangements considered have been discussed in their respective sections. Each setup is capable of obtaining good data in certain regions for specific reactions, so our choice of a specific setup becomes mostly a matter of personal preference.

2. For the systems discussed in IV (Hybrid System) and V and VI (LH_2 target), the data rates could be increased by increasing the vertical aperture of the downstream spectrometer, with a corresponding increase in cost. The magnet dimensions could reasonably be increased to 2.5 m wide × 2.5 m high × 1.5 m long, still with a

20 kG field. This change would require enlarging the downstream chambers and counters and would also require enlarging the exit aperture of the bubble-chamber system.

If the spectrometer magnet described above in Sections IV and V were purchased with dimensions 2.5 m × 1.5 m × 1.5 m, it would only be a matter of time before someone would replace the leg yokes to obtain a square aperture of 2.5 m × 2.5 m. We, therefore, strongly recommend that the coils, at least, of this magnet should be designed to provide full field at a gap of 2.5 m, even if the magnet were originally purchased with a gap of 1.5 m. The same arguments apply to other spectrometer magnets which may be considered by NAL.

3. The rapid-cycling bubble chamber can provide valuable information for certain reactions, and we urge that NAL support the development of this device.

4. We have not investigated the possibilities of using a streamer chamber around a liquid or gaseous hydrogen target; we suggest that this approach be investigated by someone during the second half of the 1969 Summer Study. The possibilities of adding a large, low-field magnet around the target spark chamber(s) should also be considered.

REFERENCES

[1] W. D. Walker, On the Use of a Hybrid Bubble Chamber in the 100-BeV Region, National Accelerator Laboratory 1968 Summer Study Report A. 3-68-100, Vol. III, p. 299.

[2] K. Strauch, Remarks on Doing Strong-Interaction Physics Involving Multiparticle Final States in the 100-BeV Region, National Accelerator Laboratory 1968 Summer Study Report C. 3-68-98, Vol. III, p. 281.

[3] H. R. Blieden et al., Brookhaven National Laboratory Proposal # 463, October 1968.

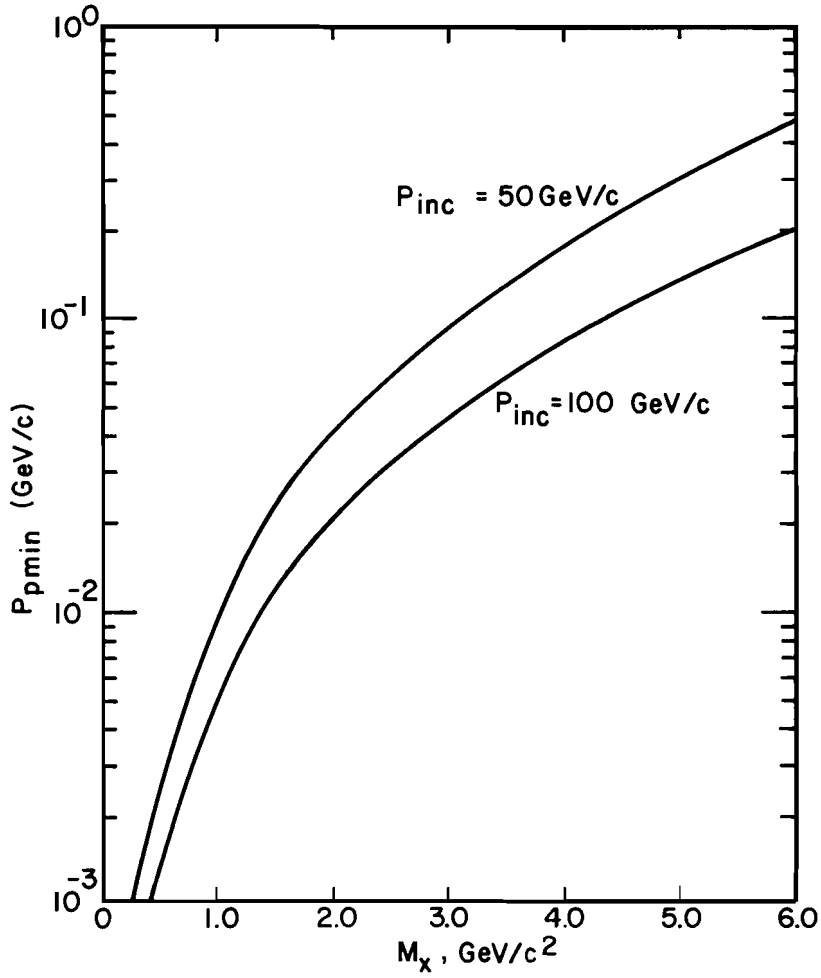

Fig. 1. Minimum proton recoil momentum in the lab vs M_x for the reaction $\pi + p \rightarrow X + p$.

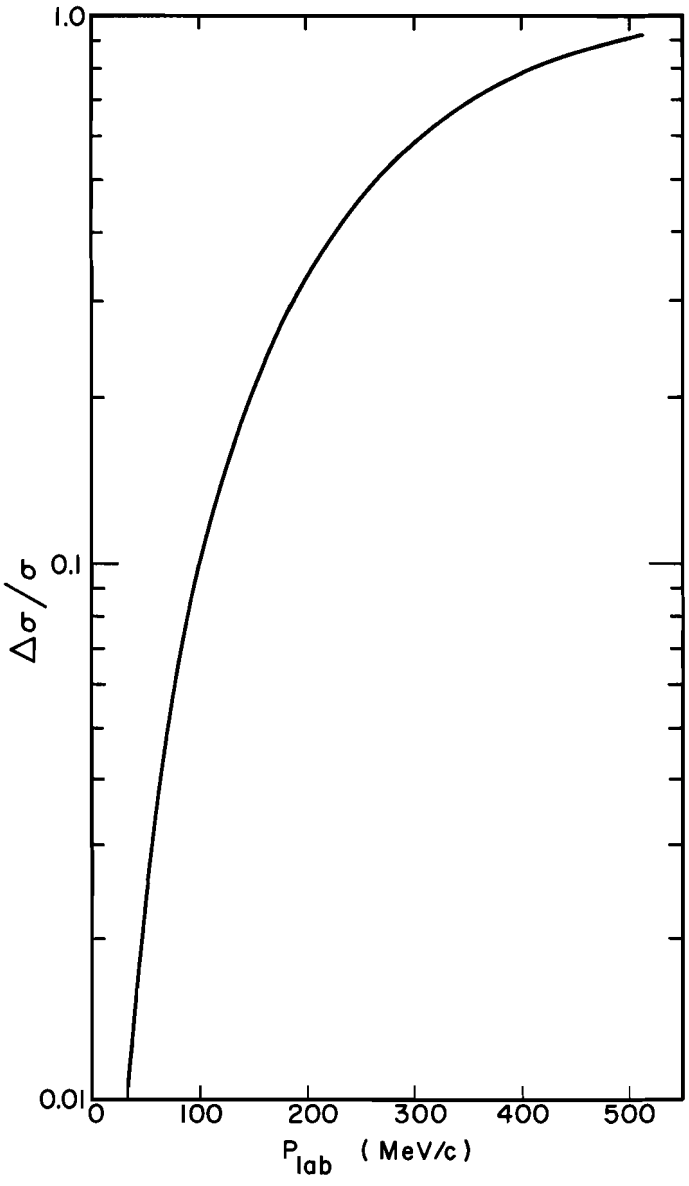

Fig. 2. $\Delta\sigma/\sigma$ vs p_{max} for the reaction $\pi + p \rightarrow X + p$. See text for definitions.

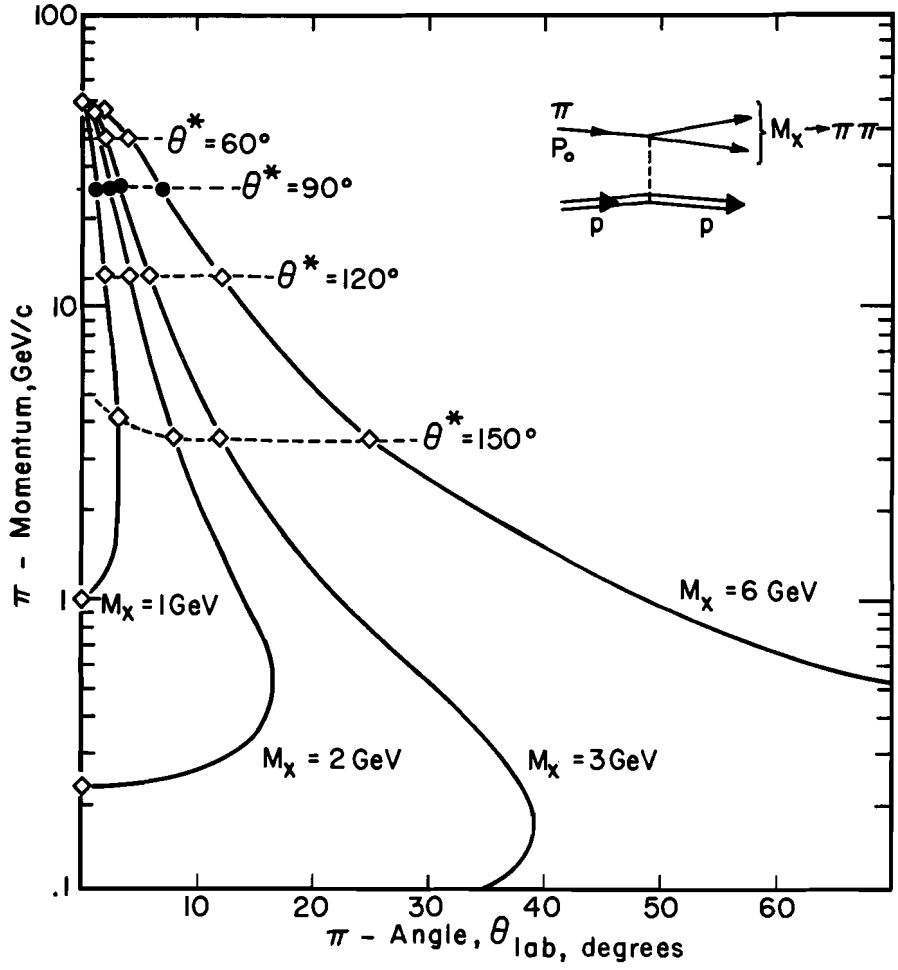

Fig. 3. Pion lab momentum vs pion lab angle for the reaction $\pi + N \rightarrow X + N$, $X \rightarrow \pi\pi$ with $p_0 = p_x = 50$ BeV/c.

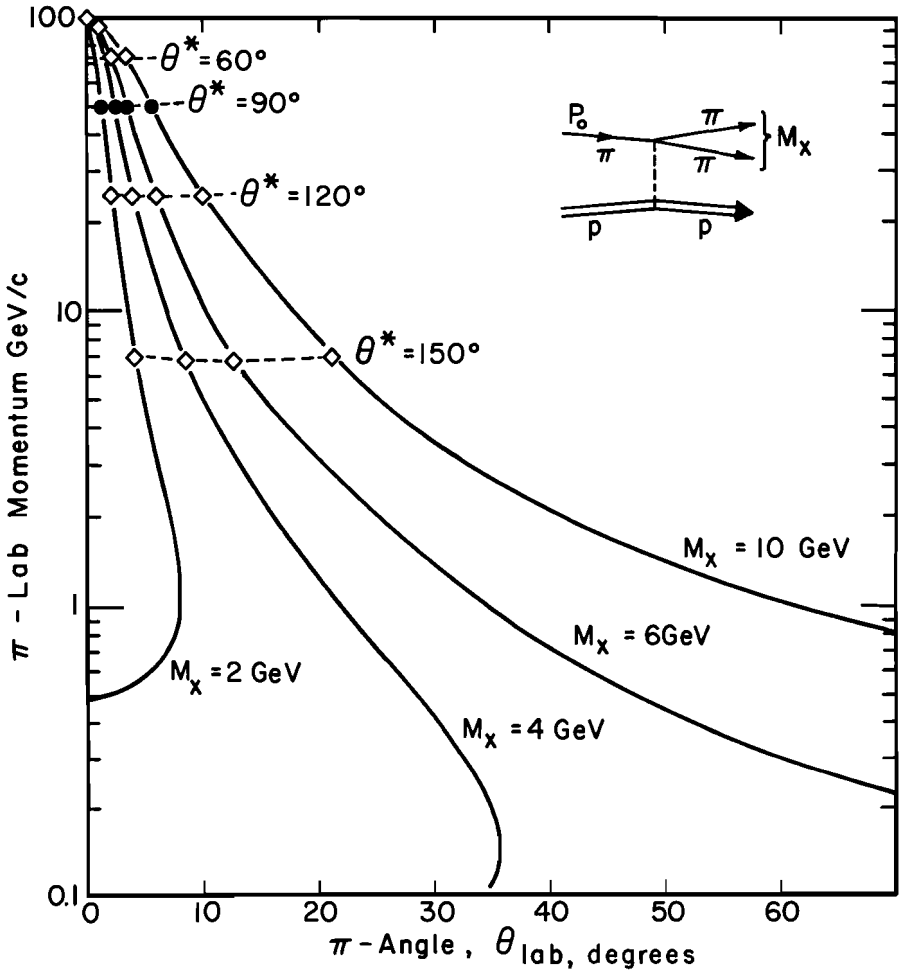

Fig. 4. Pion lab momentum vs pion lab angle for the reaction $\pi + N \rightarrow X + N$, $X \rightarrow \pi\pi$ with $p_0 = p_x = 100$ BeV/c.

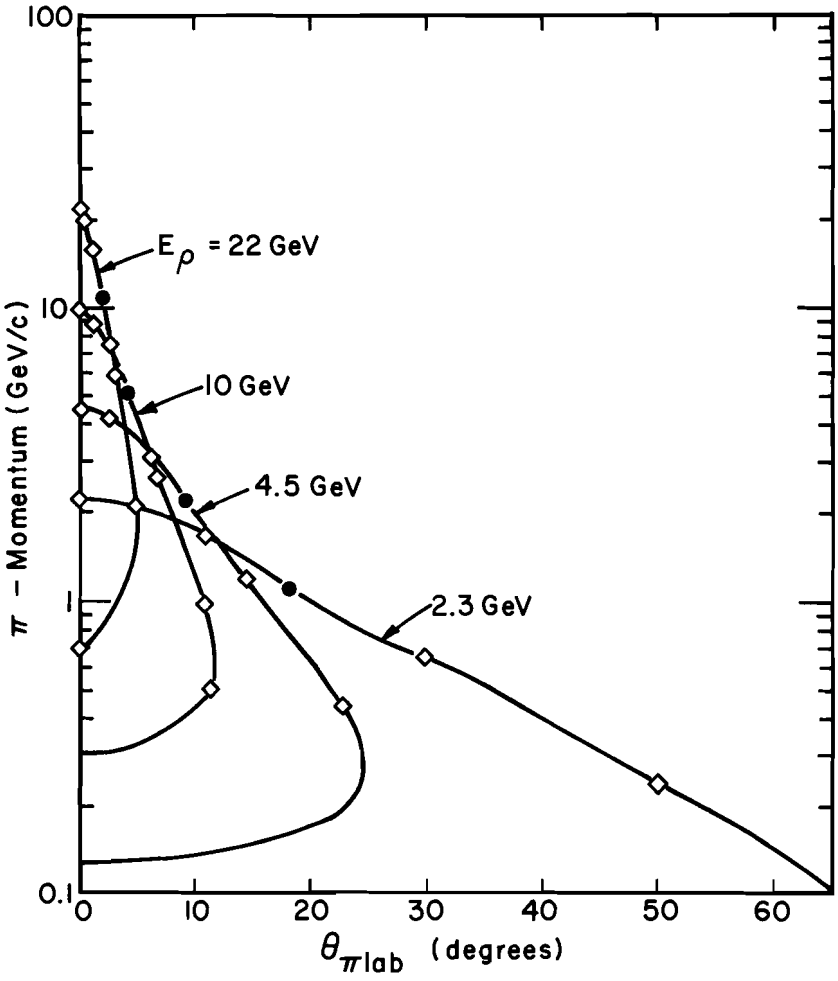

Fig. 5. Pion lab momentum vs pion lab angle for the decay $\rho \rightarrow \pi\pi$ for various ρ energies.

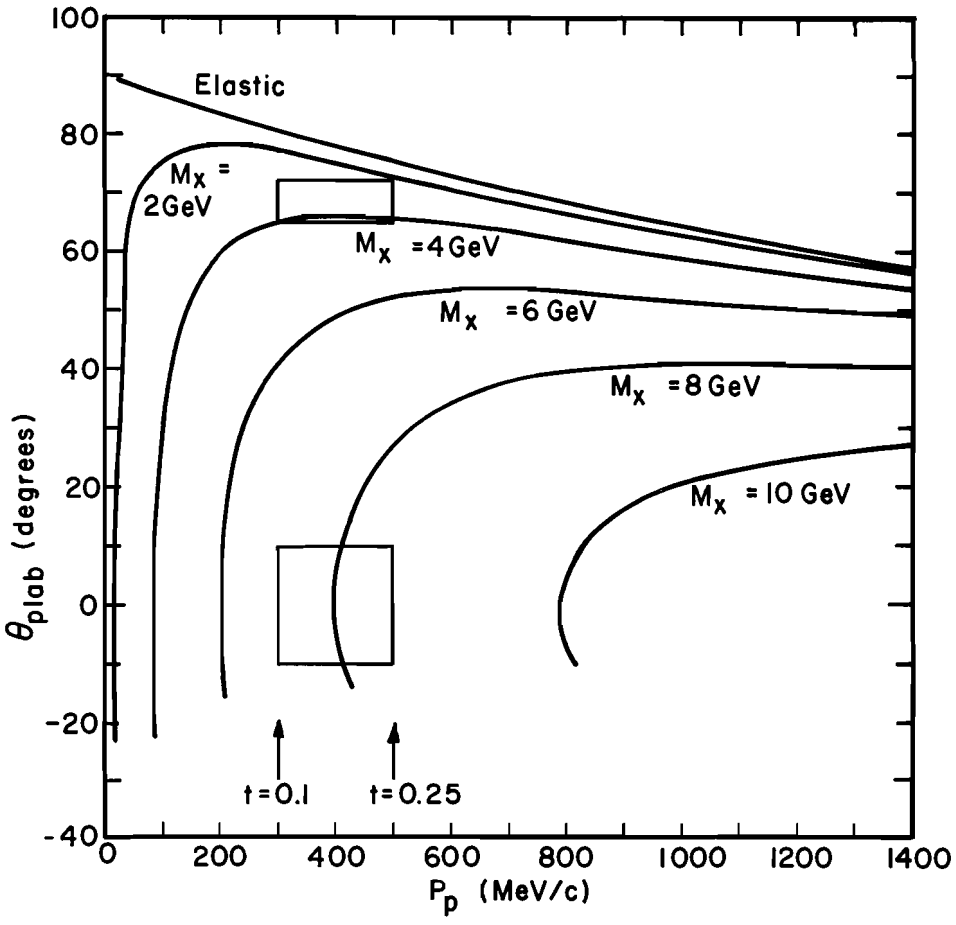

Fig. 6. Recoil proton lab angle vs proton lab momentum for $\pi + p \rightarrow X + p$.

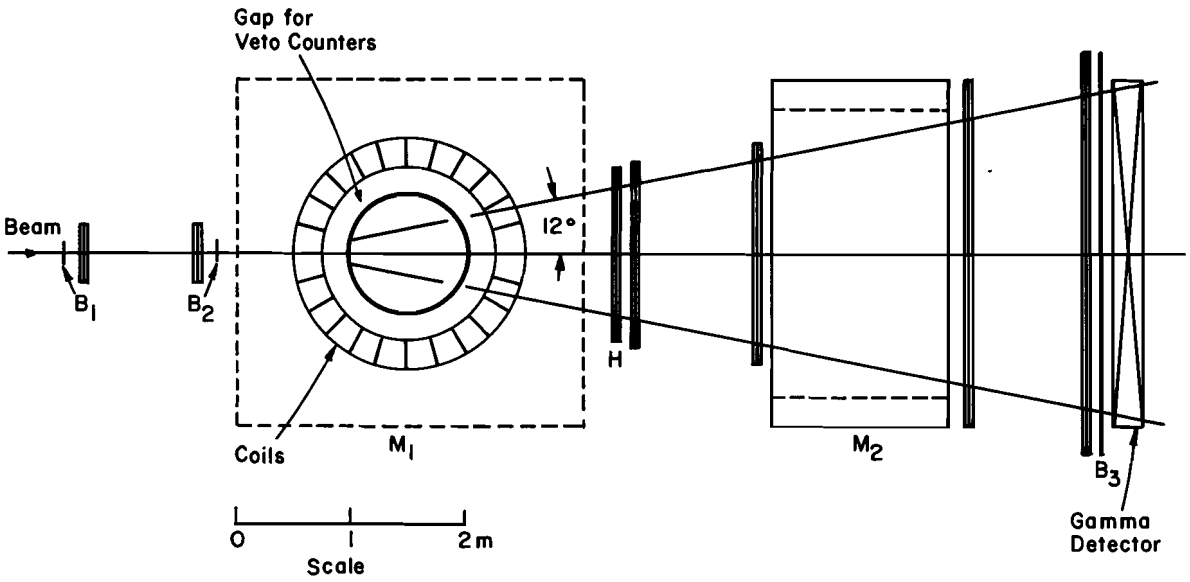

Fig. 7. Layout of hybrid system, showing the bubble chamber and downstream spectrometer.

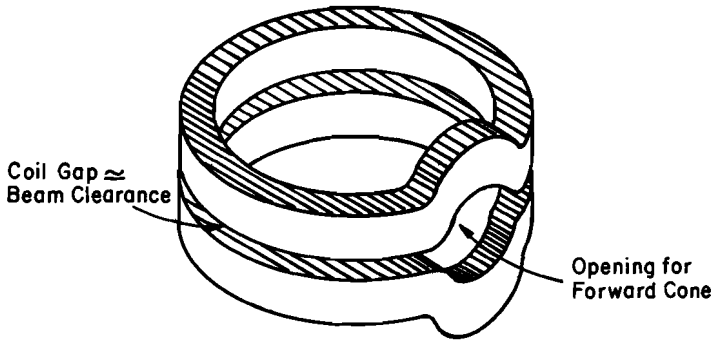

Fig. 8. Sketch of possible coil design for bubble-chamber magnet.

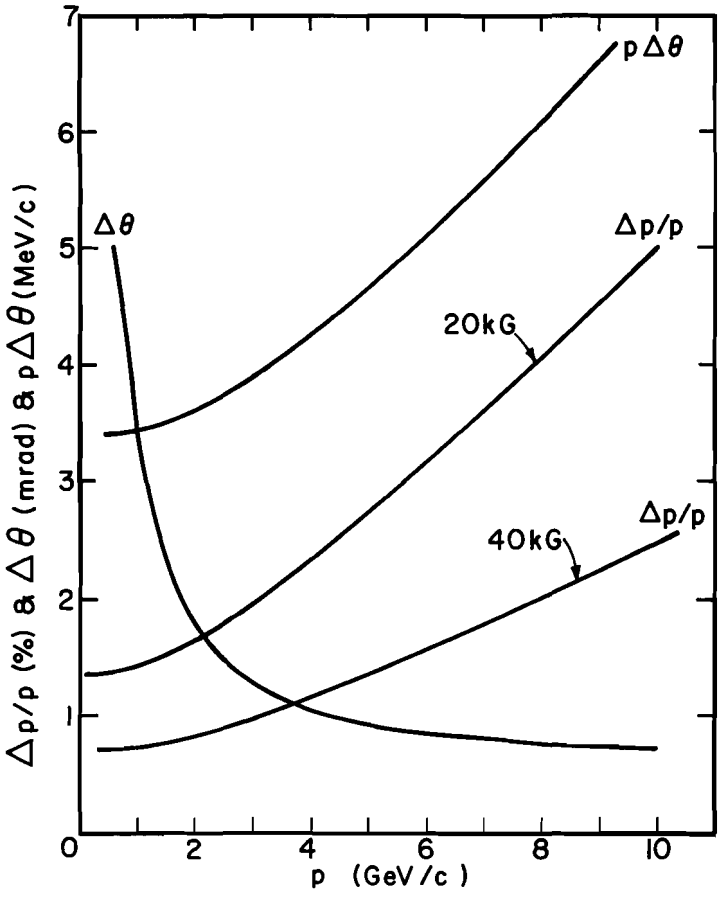

Fig. 9. Accuracy attainable in a 1 meter diameter bubble chamber with fields of 20 and 40 kG, assuming that 1/2 meter of track length is available and that the setting error is 80 microns.

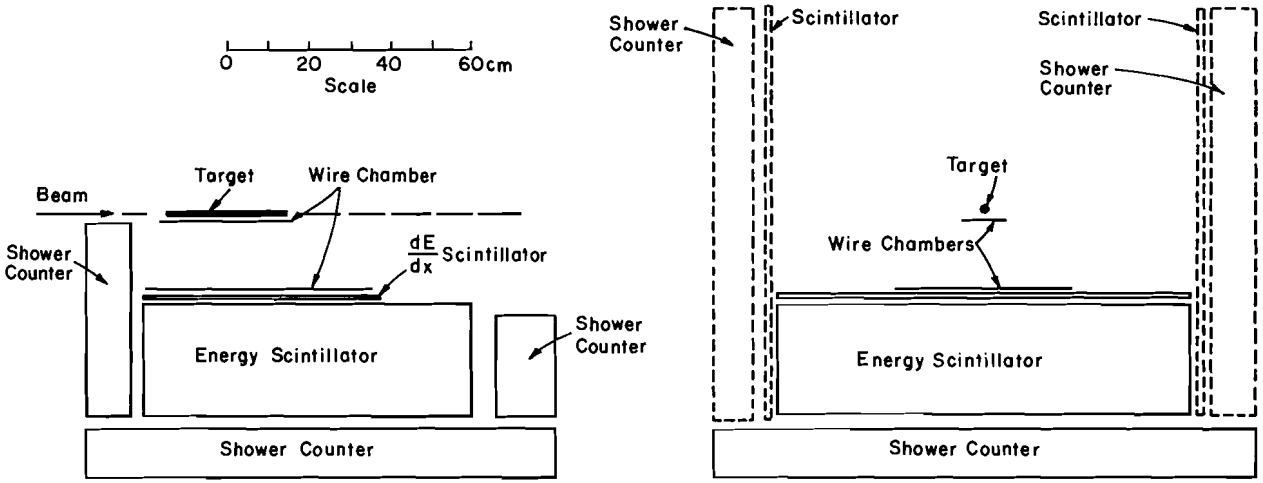

Fig. 10. Layout of liquid hydrogen target with spark chamber and counter proton detectors.

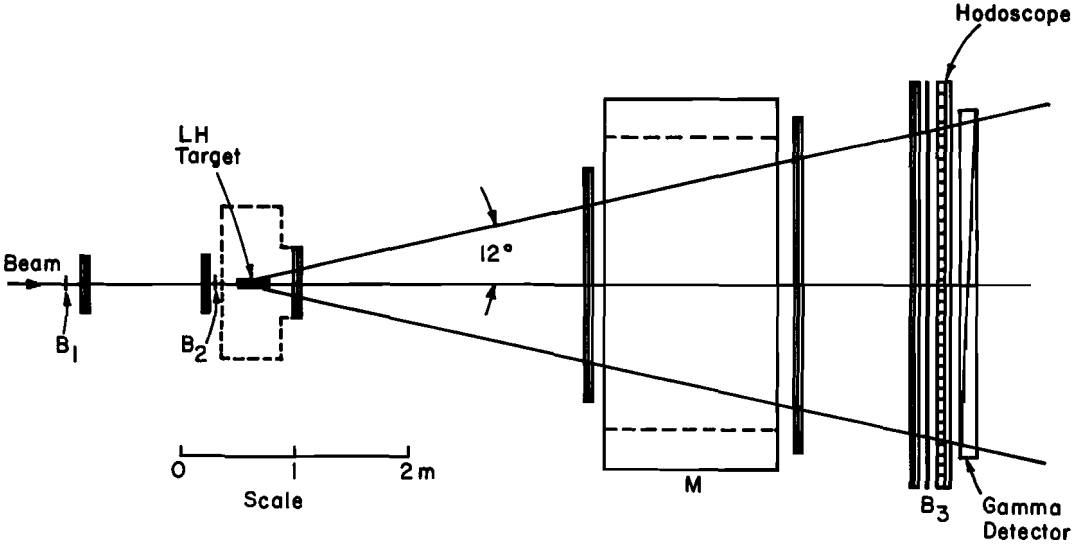

Fig. 11. Layout of LH_2 target arrangement with downstream spectrometer. See Fig. 10 for details of detectors around the target.

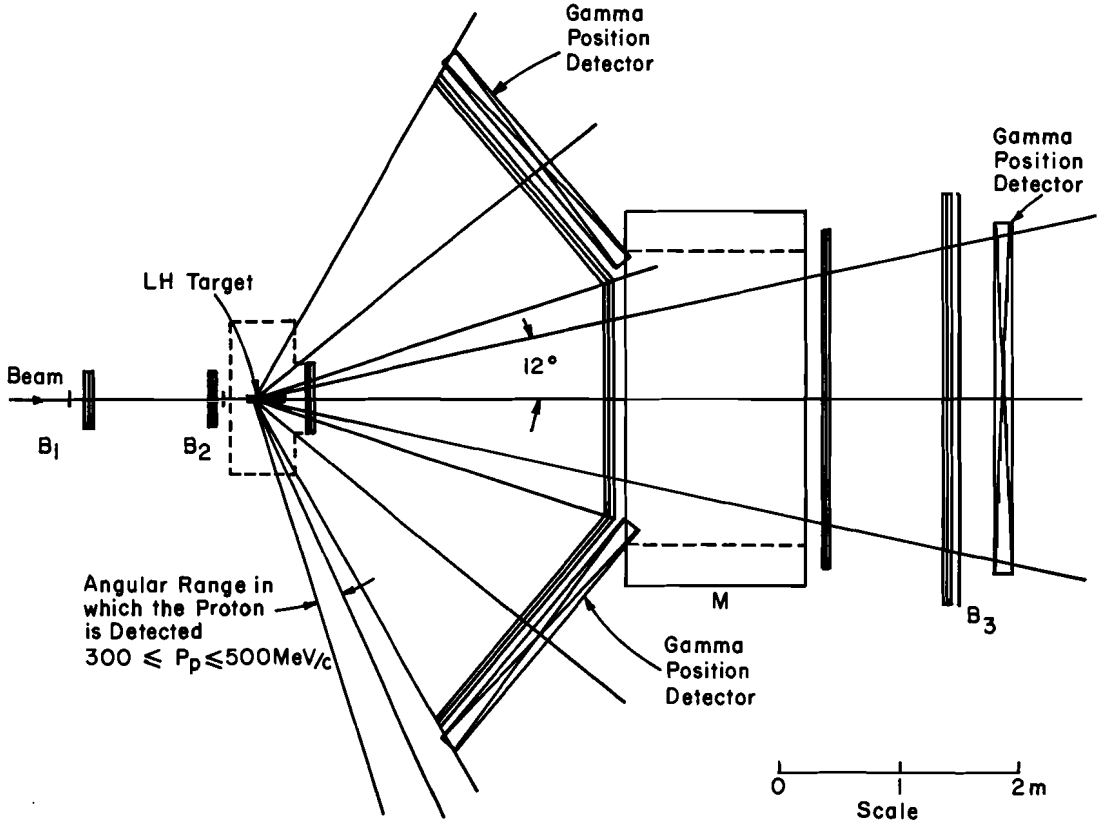

Fig. 12. Layout of a spectrometer capable of studying the whole angular distribution of the decay products of X in the reaction $\pi + p \rightarrow X + p$ at 100 BeV, $3.2 \leq M_x \leq 4.0$ BeV.